energies

MDPI

Article

Impact Analysis and Optimization of EV Charging Loads on the LV Grid: A Case Study of Workplace Parking in Tunisia

Lazher Mejdi [1,2,*], Faten Kardous [1] and Khaled Grayaa [1]

[1] National School of Advanced Sciences and Technologies of Borj Cedria (ENSTAB), University of Carthage, LR16ES08 Research Laboratory of Smart Grids and Nanotechnology (LaRINa), Hammam-Chott 1164, Tunisia
[2] Higher National School of Engineers of Tunis (ENSIT), University of Tunis, Tunis 1008, Tunisia
* Correspondence: lazhermejdi@live.fr

Abstract: With the growth of electric vehicles' (EVs) deployment as a substitute for internal combustion engine vehicles, the impact of this kind of load on the distribution grid cannot be neglected. An in-depth study needs to be performed on a regional basis to investigate the impacts of electric vehicle (EV) charging on the grid for each country's grid configuration and specifications, in order to be able to reduce them. In this work, we built a case study of a charging infrastructure of a Tunisian workplace parking lot, by combining different measured data and simulations using OpenDSS and Matlab. The first objective was to analyze the integration impacts on the Tunisian low-voltage (LV) grid including phase unbalance, voltage drop, harmonics, and power losses. We found that 10 metric tons of carbon dioxide ($MtCO_2$) in yearly emissions were caused by power losses, and 50% of these emissions came from harmonic losses, which can be avoided by active and passive filtering. The second objective was to decrease phase unbalance by formulating an optimization problem and solving it by combining a genetic algorithm (GA) and a pattern search (PS) in the Matlab environment. The GA returned interesting results by balancing the phases, and the addition of PS as a hybrid function reduced the convergence speed by 38%. Moreover, the optimization led to a reduction of 83% in the neutral current maximum value, a reduction of 67% in the violation period of the voltage drop, a minimum voltage drop of 0.94 pu. and kept the total current consumption within a fixed limit. The developed model can be adapted to any similar workplace parking facility in Tunisia that is equipped with an EV charging infrastructure.

Keywords: e-mobility; LV grid; harmonic analysis; phase balancing; power quality; genetic algorithm; pattern search

Citation: Mejdi, L.; Kardous, F.; Grayaa, K. Impact Analysis and Optimization of EV Charging Loads on the LV Grid: A Case Study of Workplace Parking in Tunisia. *Energies* **2022**, *15*, 7127. https://doi.org/10.3390/en15197127

Academic Editor: Gianpiero Colangelo

Received: 9 August 2022
Accepted: 21 September 2022
Published: 28 September 2022

1. Introduction

Global transportation has increasingly been shifting toward electrification. In the last three years (2018 to 2021), electric vehicle (EV) stock has tripled [1], which reflects the high demand for electric vehicles (EVs). As a consequence, electric vehicle supply equipment (EVSE) stock has also tripled [1]. As a matter of fact, Tunisia is not an exception from this evolution.

In fact, Tunisia has signed the Paris agreement along with the 197 other signatory countries, as a commitment to reduce greenhouse gas (GHG) emissions and achieve carbon neutrality by 2050. In this context, the Tunisian national energy management strategy aims to reinforce the energy efficiency actions, to develop renewable energies (REs) and electric mobility (e-mobility) in order to decrease emissions by approximately 22 metric tons of carbon dioxide ($MtCO_2$) by 2030, i.e., 44% of the emission of the trend scenario in comparison with 2014, which corresponds in cumulative values to 46 $MtCO_2$ over the 2014–2030 period [2]. To attain such an objective, e-mobility could help reduce polluting emissions on the road and ideally reach carbon neutral mobility when powered by REs. In this context, the Tunisian government aims to integrate about 50,000 EVs and 20,000 plug-in hybrid

electric vehicles (PHEVs) by 2025 as announced by the Tunisian National Agency for Energy Management (ANME), the head of renewable energy and e-mobility in Tunisia [3]. To reach this goal, the first ANME target will be in public transportation and public institution fleets. Moreover, the government aims to make transition from internal combustion vehicles to EVs attractive for consumers through the adoption of encouraging custom duties on EVs and PHEVs. For example, the Tunisian financial law of 2022 reduced taxes on hybrid electric vehicles (HEVs) by 50% and eliminated taxes on all types of EVs [4]. However, for a mass adoption of this technology, several barriers need to be addressed, in particular the e-mobility impact on electric grid. Indeed, many oil distribution companies have already equipped their stations with some level-2 charging points in different oil stations all over the country regardless of the electric impact on the grid [5]. Therefore, in this paper we study the EV charging impacts on the Tunisian LV grid.

In the last few years, there has been a significant global interest within the scientific community in conducting research on EV charging impact. In 2018, Deb et al. analyzed the impacts of including fast charging stations into the distribution grid by performing simulations on the 33-bus test system of the Institute of Electrical and Electronics Engineers (IEEE) for six different cases of EV charger placement. The impacts studied were voltage stability, power losses, reliability indices, and economic losses. The authors proposed a new version of an index called the voltage stability, reliability and power loss (VRP) index, which measures the EV charging impacts. This index was used, later on, as an objective function minimized with GA for the optimum placement of the charging stations [6]. Nonetheless, the proposed version of the VRP index still cannot capture the phase unbalance and the harmonics, which by itself accentuates voltage drop and power losses. In 2021, Sudha and Bollen studied the large-scale e-mobility impacts on the Swedish power grid, more specifically LV (400 V) and medium voltage (MV) (5 kV, 6 kV, 10 kV, and 20 kV) grids. They analyzed the waveform distortion, voltage dips, voltage fluctuation on light flicker, neutral, and protective earth. Their main findings about the waveform distortion included that EV charging produces harmonics, interharmonics, and supraharmonics depending on the state of charge (SoC) and the level of penetration of the EVs. For voltage drops, the authors studied its effect on the EVSE, and they found that a shallow voltage dip has no effect on the EVSE, except when it has a phase angle jump of 20° which has impacts on the EV charger and battery state of health [7]. In the same year, Ahmed et al. simulated the impacts of EV charging on both the LV (415 V) and MV (11 kV) grid in Qatar. The main focus was placed on impacts including thermal limits violation, harmonics, and the increase in electricity demand. The author found that to alleviate these impacts, a small-range EV charging infrastructure can be connected to the LV grid, whereas a large-scale infrastructure must be connected to an MV grid [8].

Other research works not only focused on the analysis of the EV charging impacts, but also proposed solutions to mitigate their effects. For instance, Turan and Gökalp proposed a simulation integrating EVSE with a grid-connected photovoltaic (PV) system at a university campus. Their aim was to mitigate the voltage drop caused by EVs' load by controlling the PV production [9]. In Turan and Gökalp's work, a PV plant installation near the EV charging infrastructure represented an interesting solution to avoid critical voltage drops. However, it did not consider PV and EVSE harmonics impacts. In a similar vein, Lo Franco et al. analyzed the peak load demand in an energy district containing PV, wind turbine, and fuel-cogeneration as sources with the support of a connection to the Italian grid and buildings, industries, householders, and EVs as loads. The purpose of this analysis was to create a prediction model of the aggregated EV load, which would be integrated in a charging management system for peak shaving [10]. Furthermore, thanks to vehicle-to-grid (V2G) and more generally vehicle-to-anything (V2X) charging services, EVs can interact with anything in the grid, which creates more flexibility for controlling the charging process and the whole energy management system. In this case, the grid can rely on the EVs' batteries in critical situations to help shaving the load peaks, regulating the voltages, balancing the phases, etc. (ancillary services) [11,12]. However, using EVs'

batteries for these services reduces their lifetime, which is undesirable for the EV users. To avoid this conflict, an electric energy storage system can be integrated in the grid and controlled by using advanced algorithms to do the job [13,14].

In this paper, we first studied the impacts of the integration of EV charging loads into the Tunisian LV grid (230 V, 400 V, 50 Hz). We specifically highlighted the harmonics and phase unbalance effects on losses and voltage dips. Afterward, we focused on reducing the phase unbalance (major impact) by solving an optimization problem with GA and PS. The paper is structured as follows. In Section 2, the materials and methods of interest are described. In Section 3, the creation of the simulation model and its input data are explained. In Section 4, the impacts of uncontrolled EV charging on the LV grid are analyzed based on the simulation model of the case study. In Section 5, phase unbalance problem is minimized by using with GA and PS.

2. Materials and Methods

2.1. Experimental Setup

In order to reduce CO_2 emissions, we are studying an RE-based e-mobility. To conduct this study, we constructed in our lab (LaRINa) an experimental setup (Figure 1), consisting of:

- Emulated power sources,
- Real PV source,
- Weather station,
- Measurement devices,
- Transmission lines, and
- Loads.

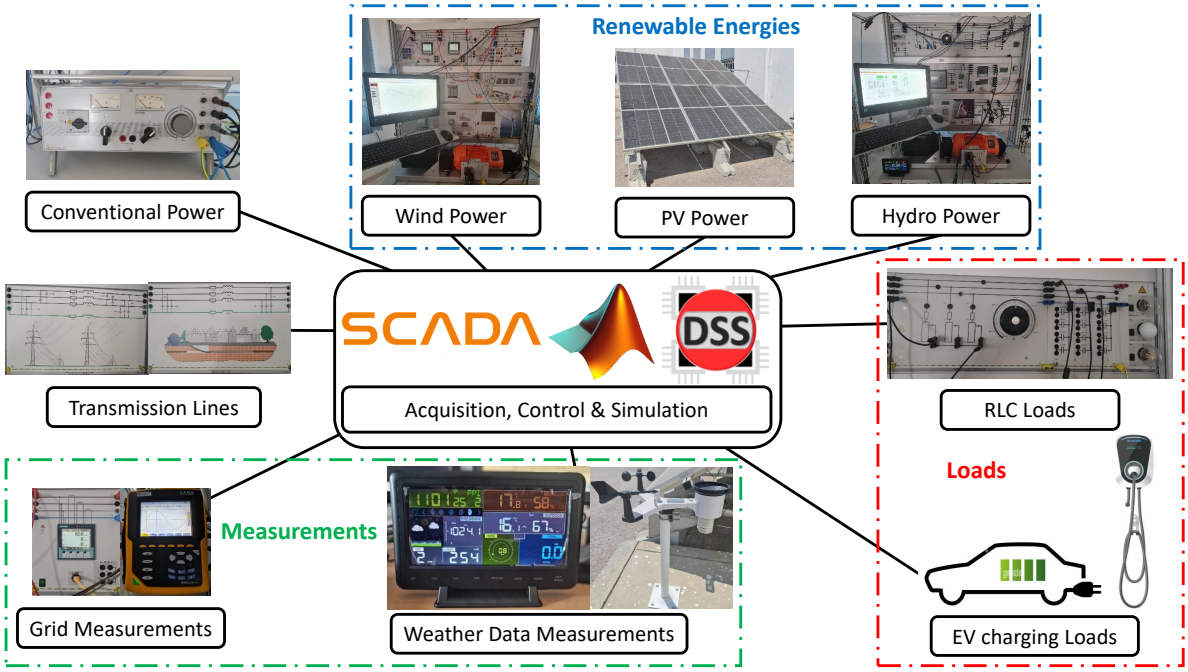

Figure 1. Available materials and tools.

The presented setup can be controlled by supervisory control and data acquisition (SCADA), Matlab, etc. In addition to these, we used in this study OpenDSS as a simulator of power distribution systems. This open-source software offers a variety of simulation modes, such as power flow, dynamic, fault study, harmonic, etc. Moreover, it can interface with many programming languages like Matlab, Python, etc. This powerful feature helps to include advanced control algorithms to manage the power distribution grid [15].

2.2. Algorithms

To solve the optimization problem, we used a genetic algorithm (GA) and pattern search (PS) in the Matlab environment.

2.2.1. Genetic Algorithm

The GA is a heuristic algorithm, widely used in many optimization problems and belongs to evolutionary algorithms [16]. Its basic format is described in Algorithm 1.

Algorithm 1 Basic genetic algorithm [16]

```
initialize population
repeat
    repeat
        crossover
        mutation
        phenotype mapping
        fitness computation
    until population complete
    selection of parental population
until termination condition
```

2.2.2. Pattern Search

Also called "Direct Search", the PS is an optimization algorithm that does not need derivative calculation for optimization. It just depends on the values of the objective function to calculate pattern vectors. From this, the algorithm will identify the point to search at each iteration [17,18]. PS can be combined with GA to achieve faster computation. For example, a small number of generation can be used combined with PS instead of 50 generations of GA to reach the same optimization results.

2.3. Data

In this work, we used data from the adaptive charging network (ACN), which is a publicly available dataset that contains information about over 30,000 charging sessions recorded in two EV charging workplace sites in California.

The dataset provides many details about each charging session that took place at these two sites from 2018 until now. These details are summarized in Table 1, and the whole dataset is available at: https://ev.caltech.edu/dataset (accessed on 21 April 2021). In addition, ACN data recorded the current consumption of these charging sessions with a timestamp of less than one second.

Table 1. ACN recorded data fields [19].

Field	Description
connectionTime	Time when the user plugs in.
doneChargingTime	Time of the last non-zero charging rate.
disconnectTime	Time when the user unplugs.
kWhDelivered	Measured Energy Delivered
siteID	Identifier of the site where the session took place.
stationID	Unique identifier of the Charging Point (CP).
sessionID	Unique identifier for the session.
timezone	Timezone for the site.
pilotSignal	Time series of pilot signals during the session.
chargingCurrent	Time series of actual charging current of the EV.
userID [1]	Unique identifier of the user.
requestedDeparture [1]	Estimated time of departure.
kWhRequested [1]	Estimated energy demand.

[1] Field not available for every session.

3. Case Study

In the absence of a large-scale EVSE-equipped car parking lot facility in Tunisia, we built our hypothetical facility by combining measured data on charging infrastructures from different sources. First, we relied on the National School of Advanced Sciences and Technologies of Borj Cedria (ENSTAB) parking architecture for the proper electric sizing of the charging infrastructure. We also took advantage of the open-source data of the ACN from Caltech [19] because it presented a case similar to what we intended to study. In addition, we measured a charging profile of one of the EVs available in the Tunisian market. We fed all these data into OpenDSS to perform dynamic and harmonic simulations. In fact, after providing OpenDSS with all the details about the grid (transformers, loads, lines, etc.), it is necessary to indicate the load profiles of the CPs, which are time series of the current consumption during the simulated period, in order to conduct the dynamic simulation. These time series are constructed by relying on sufficient knowledge about all the charging sessions taking place on each CP such as connection time, completed charging time, and the variation of the consumed current during the session. The connection time and the completed charging time information are extracted from the ACN data (more details are given in Section 3.2), and the current consumption during each session is taken from the measured charging profile (more details can be found in Section 3.3). In the next subsections, we provide a detailed description of the data we used in our conduction case study.

3.1. ENSTAB Parking

The ENSTAB has a parking lot with a maximum capacity of 74 parking spots as shown in Figure 2. To match the parking lot with the ACN data, we focused on only 54 spots (the red and orange zones). The main sources of power of the ENSTAB are two 800 kVA three-phase transformers (1.6 MVA in total). From these, 207 kVA will be allocated for the EV charging. The power is carried out through 150 mm^2 underground cable (blue line) from the transformers to the four electric cabinets (*ca1*, *ca2*, *ca3* and *ca4*), and each cabinet feeds 13 to 14 charging points (CPs) by using a 6mm^2 cable (green lines). The distance between the transformers and the farthest cabinet (*ca4*) is about 261 m.

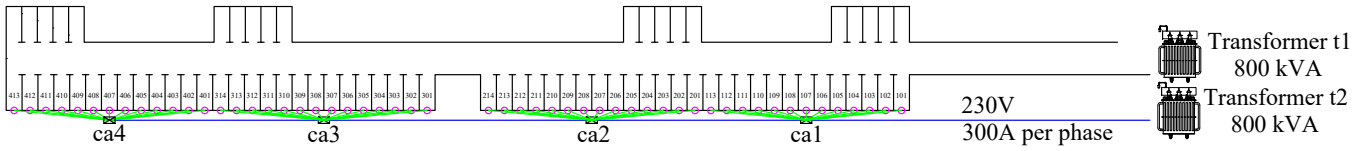

Figure 2. AutoCAD schematic of the ENSTAB parking.

Figure 3 describes the electrical diagram of the ENSTAB charging infrastructure simulated under OpenDSS. The lines that connect the main buses (*Line_STEG_ca1*, *Line_ca1_ca2*, *Line_ca2_ca3*, and *Line_ca3_ca4*) are three-phased, whereas the remaining lines (*Line_101* to *Line_413*) are single-phased. The CPs are distributed among to the three phases equally (18 CPs per phase) in such a way that *Charging Points(CPs)1* is connected to phase 1, *CP2* is connected to phase 2, *CP3* is connected to phase 3, *CP4* is connected to phase 1, and so on to the last CP.

3.2. ACN Data Extraction

We extracted two fields from the ACN data: *connectionTime* and *doneChargingTime*, to construct the events fed into the simulation model of the case study. We choose to simulate a day of events, and more specifically the day with the maximum phase unbalance. The phase unbalance can lead to many other grid problems that we want to analyze and optimize, such as network capacity waste, energy losses, neutral current rise, etc. Figure 4 shows the scenario of charging events that happened on that day. The y-axis represents

the CP number, and the color range is used to denote the current level (for our case study, the current level is usually around 32 A).

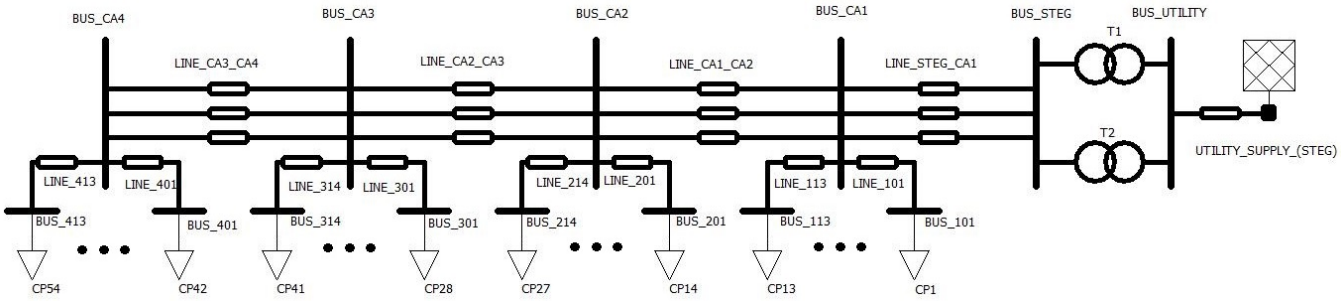

Figure 3. Electrical diagram of the ENSTAB charging infrastructure.

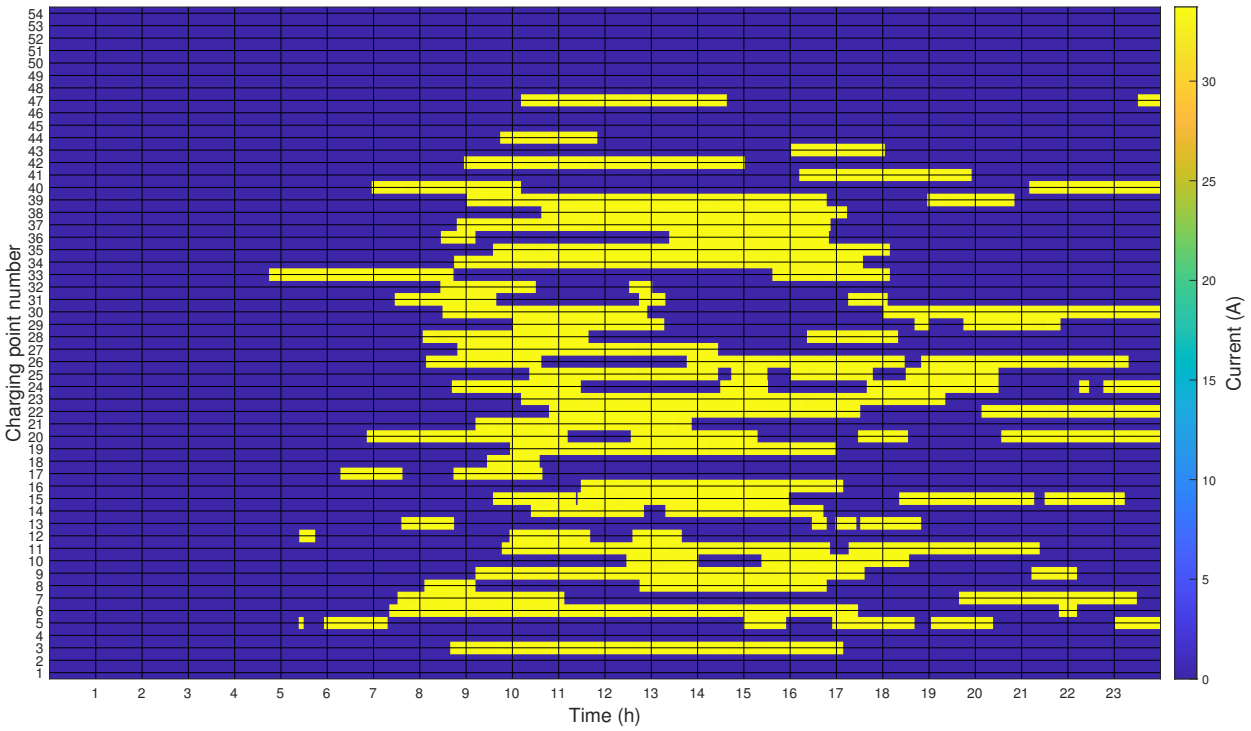

Figure 4. Charging events of the simulated day.

3.3. Charging Profile Measurement and Analysis

To integrate the EV charging load in the simulation, we measured a charging profile of an EV with its charger by using the grid analyzer C.A 8336 from Chauvin Arnoux. This EV is available in the Tunisian market.

We measured the current consumption of the EV during its charging phase from an initial SoC of 20% until full charge (the charging process stops around 96% of SoC) as shown in Figure 5. The EVSE used to charge the EV, is a level 2 single-phase AC charger SES-32-Duosida with a nominal current of 32 A (7.36 kW). For this EV, we noticed that the variation of the SoC, during the charging session, is linear. During the experience, we also visualized the current waveform for different values of pilot current (8 A, 16 A, 18 A), displayed in Figure 6. We noted a distorted shape that becomes worse if the pilot signal deceases, which reflects the increase in harmonics injection when controlling the EV charging. Furthermore, the consumed current is greater than the assigned pilot current (for example, 19.56 A consumed vs. 18 A pilot current), because of the addition of harmonics to the RMS value of the consumed current.

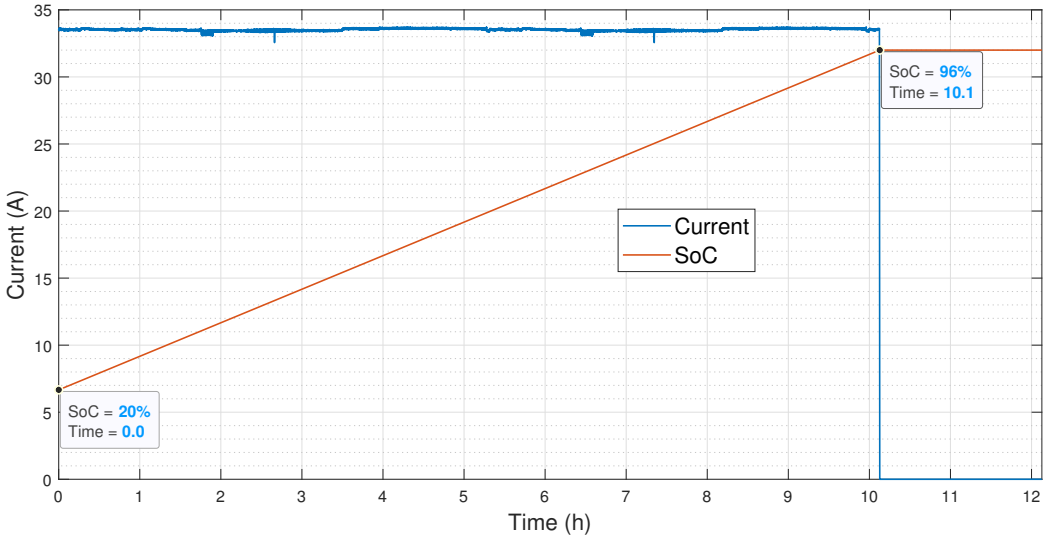

Figure 5. Measured charging profile of the EV.

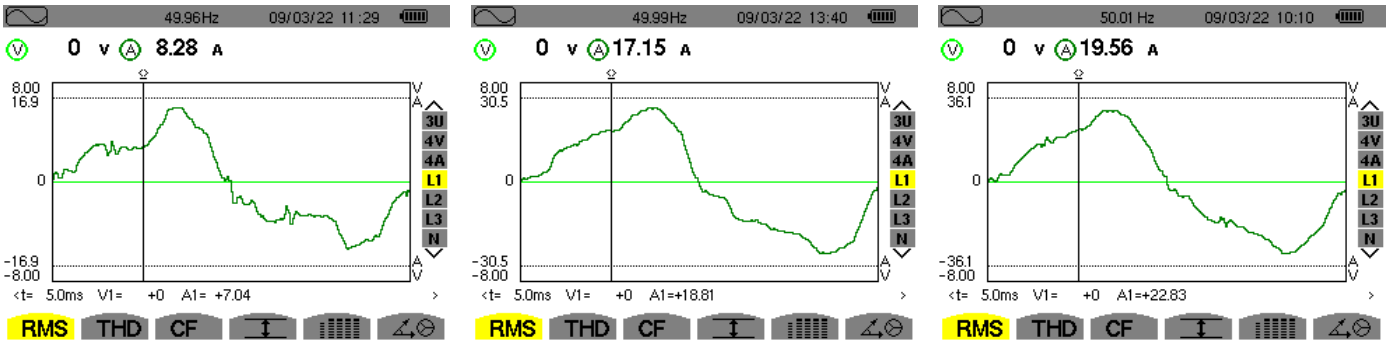

(**a**) **Pilot current of 8 A.** (**b**) **Pilot current of 16 A.** (**c**) **Pilot current of 18 A.**

Figure 6. Screenshots of the current waveform from the grid analyzer during the charging session for different pilot current values: (**a**) 8 A, (**b**) 16 A, and (**c**) 18 A.

To analyze the distorted shape of the waveform, we kept track of current harmonics variation during the charging session, which are presented in a box plot figure (Figure 7). This latter shows that the third harmonic is the most pronounced, and it ranges from 20% to 34% most of the time. Harmonics beyond the tenth are negligible compared to the nine first ones.

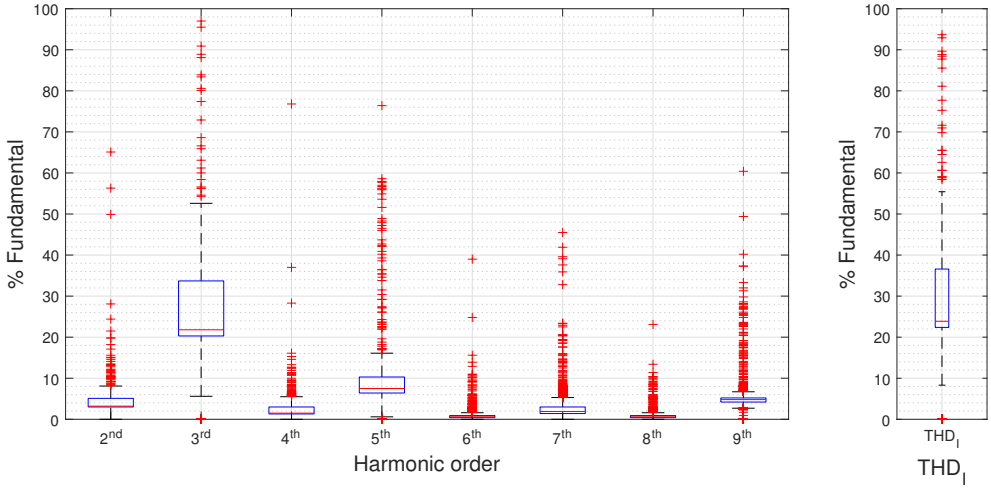

Figure 7. Current harmonics and the THD_I of the measured charging profile.

These harmonics led to a variation of the total harmonic distortion of the current (THD_I) from 22% to 37% mostly, which is defined as follows:

$$THD_I = \frac{\sqrt{\sum_{n=2}^{N} I_n^2}}{I_1}, \quad (1)$$

where I_n is the single frequency rout mean squared (RMS) value of the current at harmonic n, N is the maximum harmonic order to be considered ($N = 9$ in our case), and I_1 is the current fundamental, i.e., the RMS value of the current at 50-Hz frequency (fundamental frequency).

In the following section, we will present the simulation results of the charging infrastructure in two cases. The first one deals with uncontrolled charging, whereas the second one deals with an optimized charging used to reduce phase unbalance.

4. Impacts of Uncontrolled EV Charging on the LV Grid

Uncontrolled charging serves to denote that the EV gets the amount of power demanded at any time, and there is no power limitation or scheduling for organizing the charging sessions. This charging mode causes a lot of grid problems, including overloading, voltage drop, losses, reducing the lifetime of electrical components, phase unbalance (in case of single-phase EVSE), etc.

4.1. Phase Unbalance

Despite the fact that the CPs are unequally installed between the three phases (18 CPs per phase), phase unbalance is inevitable, because the consumer can choose freely between the available spots. In this paragraph, we will examine this unbalance in power, current, neutral current, and voltage.

4.1.1. Power Unbalance

Figure 8 shows the total power consumption of the charging infrastructure in each phase during the simulated day. It proves that the power was not distributed equally among the three phases. Furthermore, we noted an overloading of the system during a considerable amount of time. Because of this, we fixed the allocated EV charging power at 207 kVA (69 kVA per phase). For example, during 2 h, phase c is overloaded by about 20 kW.

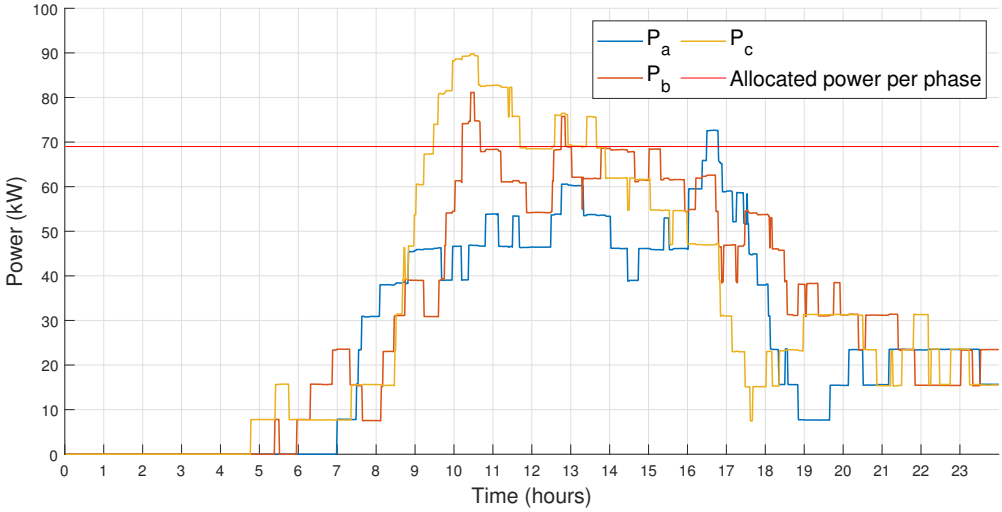

Figure 8. Total power per phase consumed by the charging infrastructure during the simulated day.

4.1.2. Current Unbalance

The phase unbalance also arose in the current consumption. Figure 9 shows the phasing unbalance index (PUI) that gives an idea about the maximum gap between the phases' current and the average current:

$$PUI[\%] = \frac{Max(|I_a - I_{avg}|, |I_b - I_{avg}|, |I_c - I_{avg}|)}{I_{avg}} \times 100, \quad (2)$$

where I_a, I_b, and I_c are the total currents in phases a, b, and c, respectively, and $I_{avg} = \frac{I_a+I_b+I_c}{3}$. This metric is used in many articles as an objective function to be minimized in order to balance phases, such as in [20–23]. The current unbalance is also exhibited by the occurrence of the none-zero neutral current (I_N).

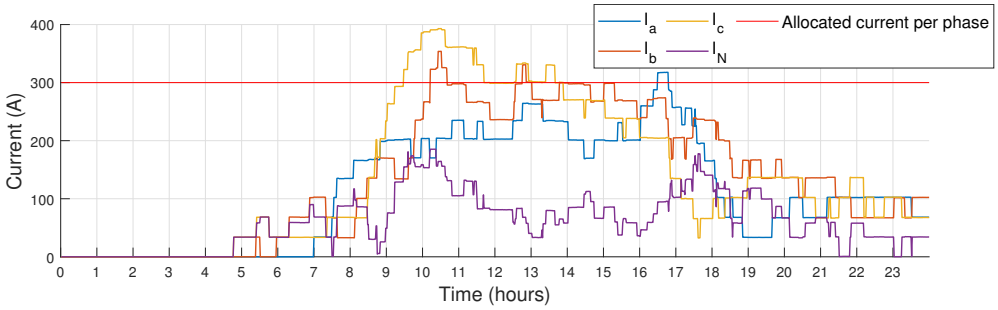

(a) Total current per phase.

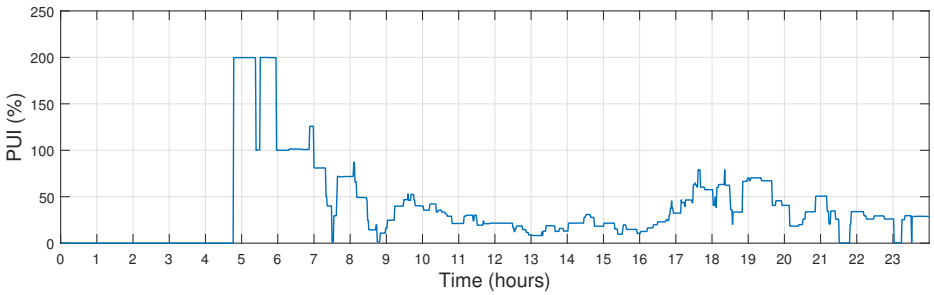

(b) PUI.

Figure 9. Total current per phase consumed by the charging infrastructure during the simulated day and the PUI. (**a**) Total current per phase and (**b**) PUI.

4.1.3. Voltage Unbalance

The voltage unbalance factor (VUF) used by the International Electrotechincal Commission (IEC) [24] captures both voltage magnitude and angle unbalance [25] according to the formula

$$VUF[\%] = \frac{|V_N|}{|V_P|} \times 100, \quad (3)$$

where

$$V_P = \frac{V_a + a.V_b + a^2.V_c}{3}, \quad (4)$$

and

$$V_N = \frac{V_a + a^2.V_b + a.V_c}{3}. \quad (5)$$

In (3), V_P and V_N are, respectively, the positive and the negative sequence voltage phasors. In (4) and (5), $a = 1\angle 120$ and V_a, V_b and V_c are the line-to-ground voltage phasors of phase a, b, and c, respectively. In our case study, the VUF can be directly calculated with OpenDSS. We focused on the four main buses (*bus_ca1*, *bus_ca2*, *bus_ca3*, and *bus_ca4*) to visualize the VUF variation during the simulated day, and the results are shown in Figure 10. According to the IEC standard [24], the VUF must not exceed 2%. Based on Figure 10, the VUF is

under the VUF standard limit in all four buses. However, the VUF in the *bus_ca4* is about to exceed the limit.

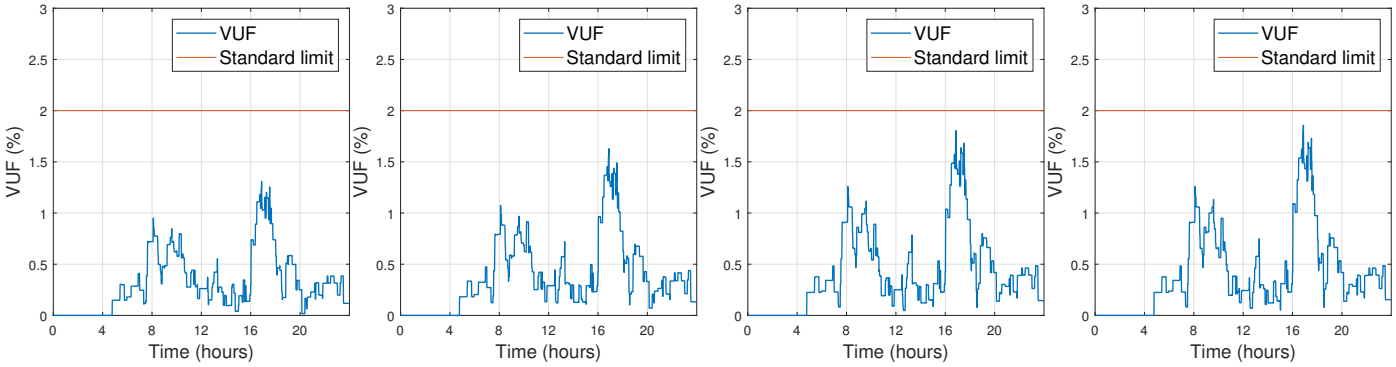

(**a**) **VUF at *bus_ca1*.** (**b**) **VUF at *bus_ca2*.** (**c**) **VUF at *bus_ca3*.** (**d**) **VUF at *bus_ca4*.**

Figure 10. The VUF variation during the simulated day at the main buses: (**a**) *bus_ca1*, (**b**) *bus_ca2*, (**c**) *bus_ca3*, and (**d**) *bus_ca4* (farthest main bus from the *bus_STEG*).

4.2. Voltage Drop

In addition to phase unbalance, EV charging can cause severe voltage drop, which can lead to the malfunctioning of electric devices. OpenDSS can get the voltages in any point of the grid at any time during the simulated day. We focused on the voltage variation at the main buses (*bus_ca1*, *bus_ca2*, *bus_ca3*, and *bus_ca4*), which is demonstrated in Figure 11. According to the IEC [24], the voltages in the LV grid must be within 0.95 and 1.05 pu. At *bus_ca1*, the voltages are barely within the standard limit. In the other buses, there is a clear violation of the lower voltage limit, which is accentuated when moving farther in the charging infrastructure (from *bus_ca2* to *bus_ca4*).

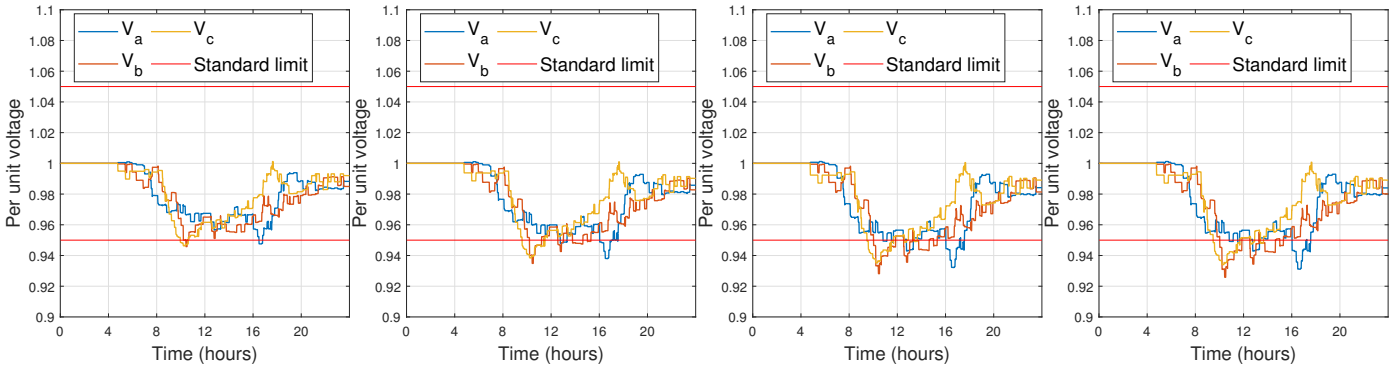

(**a**) **Voltages at *bus_ca1*.** (**b**) **Voltages at *bus_ca2*.** (**c**) **Voltages at *bus_ca3*.** (**d**) **Voltages at *bus_ca4*.**

Figure 11. Voltage variation per phase during the simulated day at the main buses: (**a**) *bus_ca1*, (**b**) *bus_ca2*, (**c**) *bus_ca3*, and (**d**) *bus_ca4* (farthest main bus from the *bus_STEG*).

4.3. Harmonics

By using the harmonic mode of OpenDSS, we performed a harmonic simulation of the charging infrastructure to analyze the current and voltage harmonics at any point of the grid. To do so, we injected the current spectrum of the CP and the voltage spectrum of the utility supply, which we measured by using the grid analyzer. In Figure 12, a box plot of the eight first harmonics are displayed along with the total demand distortion of the current TDD_I at the *bus_STEG*. The TDD_I is defined as

$$TDD_I = \frac{\sqrt{\sum_{n=2}^{N} I_n^2}}{I_L}, \quad (6)$$

where $I_L = 300A$ is maximum demand load current (fundamental frequency component) at the point of common coupling (PCC).

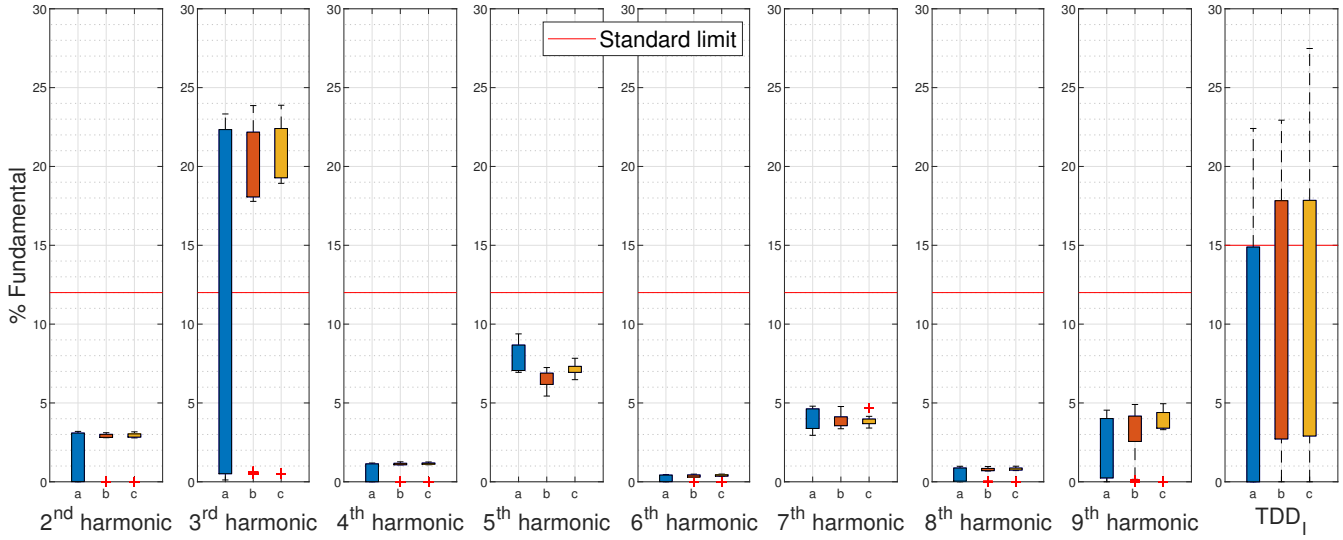

Figure 12. Current harmonics per phase injected by the charging infrastructure.

To know the standard range of the current harmonics according the IEEE 519-2014 [26], I_{sc}/I_L must be calculated, where I_{sc} is the maximum short circuit current at PCC. I_{sc} can be calculated by OpenDSS by using fault study simulation mode, which gave a value of 46,046 A. Hence, $I_{sc}/I_L \approx 153 \in [100, 1000]$; consequently, according the IEEE 519-2014 standard, each harmonic from the third until the eleventh must be less than 12%, and the TDD_I must be less than 15%. In our case, we have a violation of the standard regarding the third harmonic, and, the TDD_I exceeded 15%, especially in phases b and c.

For the voltage harmonics, we chose to visualize the harmonic content and the total harmonic distortion of the voltage THD_V at *bus_ca4*, because in the other buses, we did not find any violation of the standard. The THD_V is defined similarly to the THD_I as follows:

$$THD_V = \frac{\sqrt{\sum_{n=2}^{N} V_n^2}}{V_1}, \tag{7}$$

where V_n is the single frequency RMS value of the line-to-neutral voltage at harmonic n, and V_1 is the line-to-neutral fundamental voltage.

With reference to the IEEE 519-2014 standard [26], in the LV grid, each harmonic must not exceed 1%, and the THD_V must be less than 1.5%. According to our simulation results shown in Figure 13, the third, fifth, and THD_V are out of the standard.

4.4. Losses

The charging infrastructure is prone to different types of energy losses, such as lines losses, harmonic losses, neutral current losses, etc. The total value of the energy losses during the simulated day is the difference between the total energy consumption and the useful energy consumption (energy consumed by the CPs).

We calculated the losses for two cases, with and without harmonics, in order to know the losses caused by the harmonics. Based on the results in Table 2, the harmonic losses present 42% of the total losses. To put more emphasis on the losses due to harmonics, we performed a yearly simulation in which we used the scenario of charging events of the whole 2019 from the ACN data, and the results are shown in Table 3.

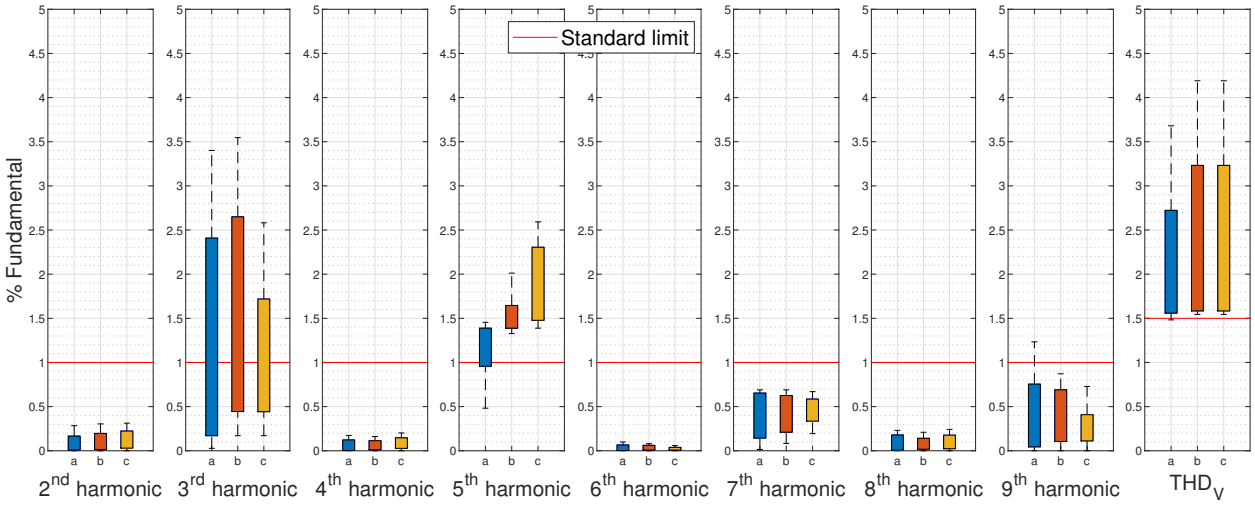

Figure 13. Voltage harmonics per phase at the *bus_ca4* (farthest main bus).

Table 2. Energy losses in the charging infrastructure.

Case	Total Energy Consumption (kVAh)	Useful Energy Consumption (kVAh)	Total Losses (kVAh)
With Harmonics	2236	2049	187
Without Harmonics	2157	2049	108
		Harmonic Losses	79 (42%)

Table 3. Yearly energy losses in the charging infrastructure.

Case	Total Energy Consumption (MVAh)	Useful Energy Consumption (MVAh)	Total Losses (MVAh)
With Harmonics	249	231	18
Without Harmonics	240	231	9
		Harmonic Losses	9 (50%)

That huge amount of harmonic loss can be reduced and even avoided with passive or active filtering, which leads to a yearly gain of CO_2 emissions of about 5.17 $MtCO_2$. The CO_2 emissions are calculated with the coefficient of the CO_2 emission per kWh of generated electricity, which is, for the case of Tunisia, 0.573 $kgCO_2/kWh$ [27].

5. Phase Balancing by Using Genetic Algorithm and Pattern Search

After presenting the results of uncontrolled charging impacts on the LV Tunisian grid, we formulated an optimization problem in order to reduce phase unbalance and overloading. To solve the problem, we first used the genetic algorithm, and then we combined it with the pattern search optimization algorithm to get better results.

5.1. Optimization Model

5.1.1. Cost Function

To decrease phase unbalance, we define a cost function that captures the gap between the power consumed in each phase:

$$\min_{I_{CP_1},\ldots,I_{CP_{54}}} \sqrt{(P_a - P_b)^2 + (P_b - P_c)^2 + (P_c - P_a)^2}, \quad (8)$$

where P_a, P_b and P_c are the total amount of power consumed in phases a, b, and c, respectively, and I_{CP_1}, ..., $I_{CP_{54}}$ are the currents consumed by the 54 CPs.

5.1.2. Constraints

We also wanted to reduce overloading; therefore, we limited the total current consumed in each phase by I_L, as intended when sizing the charging infrastructure. This constraint is expressed in (9),

$$A.I \leq b, \tag{9}$$

where

$$A = \left(\begin{pmatrix} 1 & 0 & 0 \\ 0 & 1 & 0 \\ 0 & 0 & 1 \end{pmatrix} \dots \begin{pmatrix} 1 & 0 & 0 \\ 0 & 1 & 0 \\ 0 & 0 & 1 \end{pmatrix} \right) \textit{ is a } 3 \times 54 \textit{ matrix}, I = \begin{pmatrix} I_{CP_1} \\ \vdots \\ I_{CP_{54}} \end{pmatrix} \textit{ and } b = \begin{pmatrix} I_L \\ I_L \\ I_L \end{pmatrix}. \tag{10}$$

5.1.3. Implementation by Using Matlab and OpenDSS

In our work, we used Matlab–OpenDSS interfacing to optimize the charging infrastructure. The optimization process is explained in Algorithm 2, where, *Optimize* is a Matlab function that deals, in our case, with minimizing the cost function at a certain time and *Simulate* launches the simulation of the infrastructure at a certain time.

Algorithm 2 Optimization process

for $t = 1$ to 1440 do ▷ Loop over a day with a timestamp of 1 min
  if $phaseUnbalance = True$ **then**
    repeat
      $I^*_{CP_1}(t), ..., I^*_{CP_{54}}(t) \leftarrow Optimize(I_{CP_1}(t), ..., I_{CP_{54}}(t))$
      $P_a(t), P_b(t), P_c(t) \leftarrow Simulate(I^*_{CP_1}(t), ..., I^*_{CP_{54}}(t))$
      $costFunction(t) \leftarrow \sqrt{(P_a(t) - P_b(t))^2 + (P_b(t) - P_c(t))^2 + (P_c(t) - P_a(t))^2}$
    until $numberOfGeneration = 35$ **and** $fitnessValue = 0.1$
  else
    $I^*_{CP_1}(t), ..., I^*_{CP_{54}}(t) \leftarrow I_{CP_1}(t), ..., I_{CP_{54}}(t)$
  end if
  $finalResults(t) \leftarrow Simulate(I^*_{CP_1}(t), ..., I^*_{CP_{54}}(t))$
end for

5.2. Algorithms Convergence Efficiency

In order to show the efficiency of the used algorithms, Figure 14 displays an example of the optimization with GA from the simulated day. Based on the plot of the fitness value, 50 generations are sufficient to reach an acceptable minimum. Furthermore, in Figure 15, the same example is shown, but we added PS as a hybrid function. We compared 36 generations of the GA result with only 15 generations combined with PS. In the two cases, it reached the same final fitness value; however, the first case took 25.3 s to converge, and the second case took only 15.8 s. Consequently, GA combined with PS is 9.5 s faster (38% less time than GA).

5.3. Optimization Results and Discussion

In Figure 16, the effects of the optimization on current unbalance, neutral current, and the PUI are displayed. The GA has already achieved promising results. However, we continued the optimization process to see what the PS can add. For the results of GA, the current unbalance was significantly reduced, and the neutral current went down from a maximum of 180 A, for the case of uncontrolled charging, to 40 A. When GA and PS were combined, the current unbalance almost vanished and the neutral current remained at zero level for most of the day and the maximum value became 30 A. In summary, the maximum value of the neutral current decreased by 78% thanks to GA and by 83% during the GA and

PS combination. Regarding the PUI, it decreased with GA and became almost zero when using GA and PS except between 5:00 and 7:00. Only one or two charging sessions took place, i.e., $\{I_a = 32$ A and $I_b = I_c = 0\}$ or $\{I_a = I_b = 32$ A and $I_c = 0\}$. Therefore, the PUI will be either 200% or 100% as explained below:

- In the first case, $I_{avg} = 10.7$ A and the PUI (defined in (2)) will be $PUI = \frac{Max(|I_a - I_{avg}|, |I_b - I_{avg}|, |I_c - I_{avg}|)}{I_{avg}} \times 100 = \frac{Max(|32-10.7|, |0-10.7|, |0-10.7|)}{10.7} \times 100 \approx 200\%$
- In the second case, $I_{avg} = 21.3$ A and the PUI will be $PUI = \frac{Max(|I_a - I_{avg}|, |I_b - I_{avg}|, |I_c - I_{avg}|)}{I_{avg}} \times 100 = \frac{Max(|32-21.3|, |32-21.3|, |0-21.3|)}{21.3} \times 100 \approx 100\%$.

In these two cases, no phase balancing can be done. For the other part of the simulated day, the PUI went down from a maximum value of 125% to 50% with GA (60% reduction) and to 35% with GA and PS combination (72% reduction). Concerning overloading, GA already kept all the currents under the desired maximum limit (300 A), which was 390 A before optimization (23% reduction).

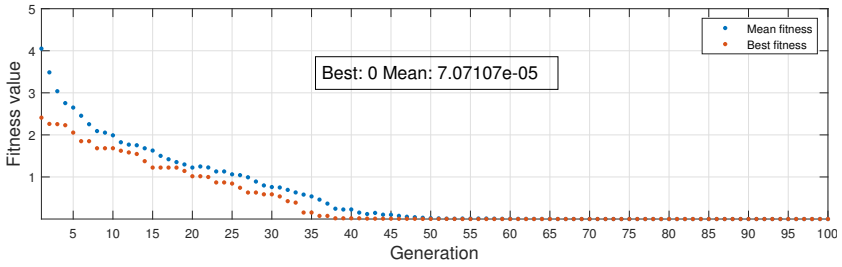

(**a**) **Fitness value.**

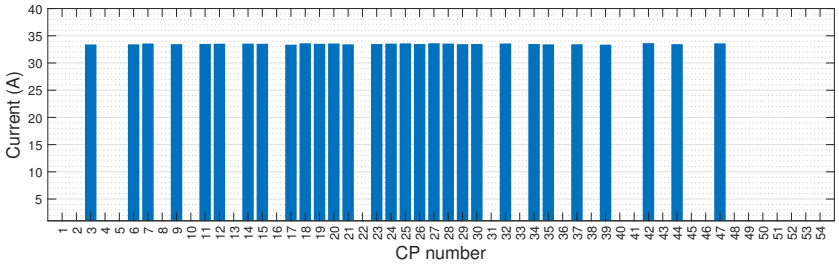

(**b**) **Initial individual.**

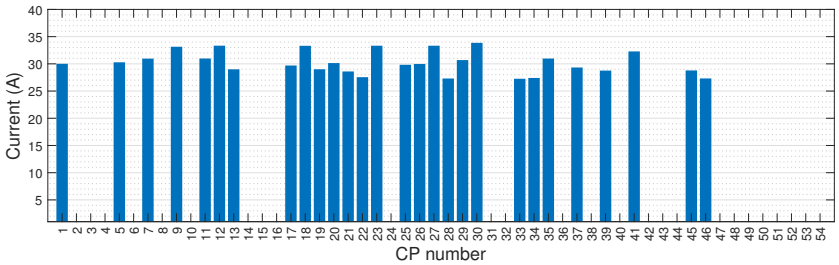

(**c**) **Best individual.**

Figure 14. Convergence plots of GA. (**a**) Fitness value. (**b**) Initial individual. (**c**) Best individual.

Figure 17 shows what happened to the voltage drop, voltage unbalance, and the VUF after optimization at the bus *ca4*. The voltage unbalance is reduced with GA, and even a bit more when adding PS. The voltage drop was under the limit from 9:00 until 18:00 reaching, in some moments, 0.93 pu before optimization. By using GA, the limit violation is reduced within 10:00 and 14:00, and when adding PS, it decreased the violation period by another hour. Moreover, the minimum voltage drop became 0.94 pu. In summary, the violation period decreased by 5 h with GA (56% reduction) and 6 h with the GA and PS combination (67% reduction), and for both cases' violation the value is 0.94 pu. Regarding

the VUF, before optimization, there was not any violation of the standard limit, but even though the GA alone, and when combined with PS, decreased the VUF significantly. Hence, there will be no problem keeping the VUF within the standard in the worst cases of phase unbalance.

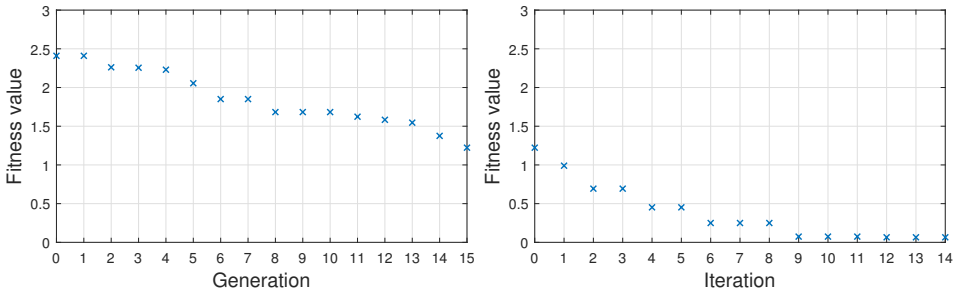

(**a**) **Convergence speed of GA.** (**b**) **Convergence speed of PS.**

Figure 15. Convergence speed of combined GA & PS. (**a**) Convergence speed of GA. (**b**) Convergence speed of PS.

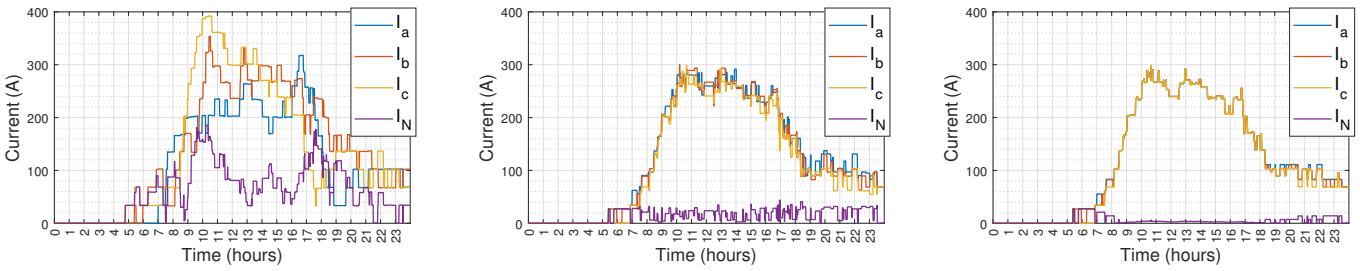

(**a**) **Total currents and neutral current without optimization.**

(**b**) **Total currents and neutral current optimized with GA.**

(**c**) **Total currents and neutral current optimized with combined GA & PS.**

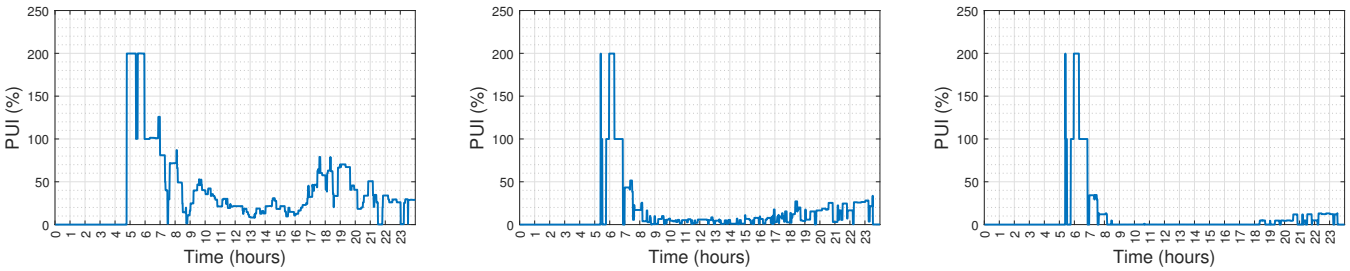

(**d**) **PUI without optimization.**

(**e**) **PUI optimized with GA.**

(**f**) **PUI optimized with combined GA & PS.**

Figure 16. Total currents, neutral current, and the PUI for three cases. (**a**) Total currents and neutral current without optimization. (**b**) Total currents and neutral current optimized with GA. (**c**) Total currents and neutral current optimized with combined GA and PS. (**d**) PUI without optimization. (**e**) PUI optimized with GA. (**f**) PUI optimized with combined GA and PS.

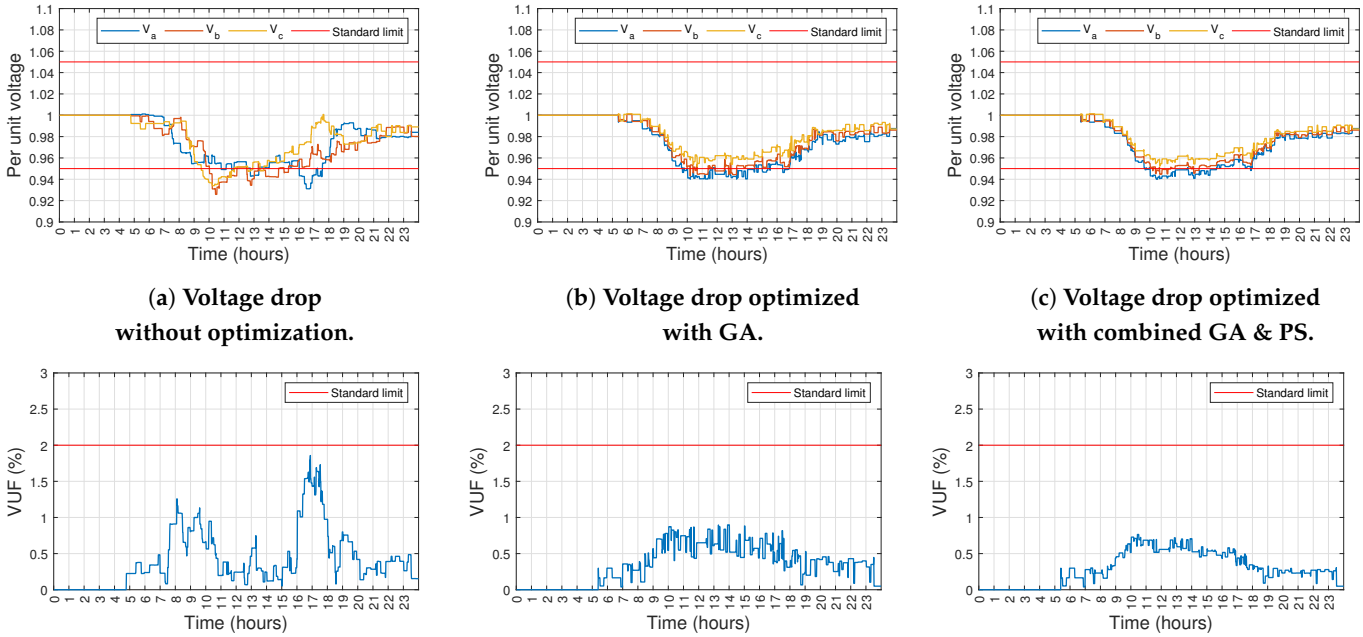

(a) Voltage drop without optimization. **(b) Voltage drop optimized with GA.** **(c) Voltage drop optimized with combined GA & PS.**

(d) VUF without optimization. **(e) VUF optimized with GA.** **(f) VUF optimized with combined GA & PS.**

Figure 17. Voltage drop and the VUF at the bus ca4 for three cases. (**a**) Voltage drop without optimization. (**b**) Voltage drop optimized with GA. (**c**) Voltage drop optimized with combined GA & PS. (**d**) VUF without optimization. (**e**) VUF optimized with GA. (**f**) VUF optimized with combined GA & PS.

6. Conclusions

In this paper, we proposed a model of a charging infrastructure based on real measured data and by using OpenDSS and Matlab. This model was implemented for an LV distribution system of a university parking lot, aiming to analyze the impacts of EV charging on the LV grid in the Tunisian context. One of the major impacts was phase unbalance, so we formulated an optimization problem to reduce this impact by combining GA and PS to solve the problem. Moreover, EV charging induced an out-of-standard voltage drop that may harm the distribution transformer, the EVSE, and the other LV grid components. Regarding the power quality, CPs produced a very important number of harmonics (mostly the third harmonic for our CP) that affect the power quality at the PCC, which means a lower quality for the other consumers. In addition, these harmonics caused yearly losses of 9 MVAh, which is equivalent to 5.17 $MtCO_2$ emission. However, the harmonics problem can be less pronounced when the charging infrastructure is equipped with EVSE from different manufacturers, because of the harmonic cancellation effect [28]. The optimization process using GA and PS led to interesting results, not only for the phase unbalance (83% reduction in the maximum value of the neutral current), but also for helping to reduce the voltage drop and keeping the current consumption under the limit. In fact, the violation period of the voltage drop is reduced by 67%. Regarding the current maximum limit, its value dropped from 390 A per phase to 300 A. As a perspective on this work, a more sophisticated optimization problem needs to be formulated with more real systems included (REs) and solved with different algorithms (machine learning, reinforcement learning, etc.), in order to address more EV charging impacts, especially power quality.

Author Contributions: Conceptualization, L.M. and K.G.; Data curation, L.M.; Formal analysis, F.K. and K.G.; Funding acquisition, L.M.; Investigation, F.K. and K.G.; Methodology, F.K. and K.G.; Project administration, K.G.; Resources, L.M.; Software, L.M.; Supervision, F.K. and K.G.; Validation, F.K. and K.G.; Visualization, L.M.; Writing—original draft, L.M.; Writing—review & editing, F.K. and K.G. All authors have read and agreed to the published version of the manuscript.

Funding: This work was supported by the German Academic Exchange Service (DAAD), Federal Ministry for Economic Cooperation and Development (BMZ), Germany, within the framework of the REMO project (Renewable Energy-based E-Mobility in Higher Education) ID 57545562.

Institutional Review Board Statement: Not applicable.

Informed Consent Statement: Not applicable.

Data Availability Statement: This work used the publicly available data of the Adaptive Charging Network [19], which can found in https://ev.caltech.edu/dataset (accessed on 21 April 2021).

Conflicts of Interest: The authors declare no conflict of interest.

References

1. IEA. *Global Electric Vehicle Outlook 2022*; Technical Report; IEA: Paris, France, 2022.
2. ANME. *National Energy Management Strategy: Objectives, Means and Challenges*; Technical report; National Agency for Energy Management (ANME): Tunis, Tunisia, 2014.
3. *Energetic and Ecological Transition in Tunisia on the Horizon of 2050*; Tunisian Institute for Strategic Studies : Tunis, Tunisia, 2022.
4. *Decree-Law No. 2021-21 of December 28, 2021, on the Finance Law for the Year 2022*; Tunisian Ministry of Finances: Tunis, Tunisia, 2021.
5. Number of EV Chargers Installed by Total Energies. 2022. Available online: https://services.totalenergies.tn/reseau-de-bornes-de-recharges-electriques (accessed on 8 August 2022).
6. Deb, S.; Tammi, K.; Kalita, K.; Mahanta, P. Impact of electric vehicle charging station load on distribution network. *Energies* **2018**, *11*, 178. [CrossRef]
7. Sudha, L.S.; Bollen, M. *Impact of Electric Vehicle Charging on the Power Grid*; Technical report; Lulea University of Technology: Lulea, Sweden, 2021.
8. Ahmed, A.; Iqbal, A.; Khan, I.; Al-Wahedi, A.; Mehrjerdi, H.; Rahman, S. Impact of EV charging station penetration on harmonic distortion level in utility distribution network: A case study of Qatar. In Proceedings of the 2021 IEEE Texas Power and Energy Conference (TPEC), virtually, 2–5 February 2021; pp. 1–6.
9. Turan, M.T.; Gökalp, E. Integration Analysis of Electric Vehicle Charging Station Equipped with Solar Power Plant to Distribution Network and Protection System Design. *J. Electr. Eng. Technol.* **2022**, *17*, 903–912. [CrossRef]
10. Lo Franco, F.; Ricco, M.; Mandrioli, R.; Grandi, G. Electric vehicle aggregate power flow prediction and smart charging system for distributed renewable energy self-consumption optimization. *Energies* **2020**, *13*, 5003. [CrossRef]
11. Canevese, S.; Cirio, D.; Gallanti, M.; Gatti, A. Ev flexibility supply via participation in balancing services: Possible profitability for italian end users. In Proceedings of the 2019 AEIT International Annual Conference (AEIT), Florence, Italy, 18–20 September 2019; pp. 1–6.
12. Thompson, A.W.; Perez, Y. Vehicle-to-Everything (V2X) energy services, value streams, and regulatory policy implications. *Energy Policy* **2020**, *137*, 111136. [CrossRef]
13. Smolenski, R.; Szczesniak, P.; Drozdz, W.; Kasperski, L. Advanced metering infrastructure and energy storage for location and mitigation of power quality disturbances in the utility grid with high penetration of renewables. *Renew. Sustain. Energy Rev.* **2022**, *157*, 111988. [CrossRef]
14. Grobelna, I.; Szcześniak, P. Interpreted Petri Nets Applied to Autonomous Components within Electric Power Systems. *Appl. Sci.* **2022**, *12*, 4772. [CrossRef]
15. Dugan, R.C.; Montenegro, D. *OpenDSS Manual Reference Guide the Open Distribution System Simulator (OpenDSS)*; Electric Power Research Institute: Palo Alto, CA, USA, 2022.
16. Kramer, O. Genetic algorithms. In *Genetic Algorithm Essentials*; Springer: 2017; pp. 11–19.
17. Lewis, R.M.; Torczon, V.; Trosset, M.W. Direct search methods: Then and now. *J. Comput. Appl. Math.* **2000**, *124*, 191–207. [CrossRef]
18. Madić, M.; Radovanović, M. Optimization of machining processes using pattern search algorithm. *Int. J. Ind. Eng. Comput.* **2014**, *5*, 223–234. [CrossRef]
19. Lee, Z.; Li, T.; Low, S.H. ACN-Data: Analysis and Applications of an Open EV Charging Dataset. In Proceedings of the Tenth International Conference on Future Energy Systems, Phoenix, AZ, USA, 25–28 June 2019.
20. Lin, C.H.; Chen, C.S.; Chuang, H.J.; Ho, C.Y. Heuristic rule-based phase balancing of distribution systems by considering customer load patterns. *IEEE Trans. Power Syst.* **2005**, *20*, 709–716. [CrossRef]
21. Huang, M.Y.; Chen, C.S.; Lin, C.H.; Kang, M.S.; Chuang, H.J.; Huang, C.W. Three-phase balancing of distribution feeders using immune algorithm. *IET Gener. Transm. Distrib.* **2008**, *2*, 383–392. [CrossRef]
22. Gupta, N.; Swarnkar, A.; Niazi, K. A novel strategy for phase balancing in three-phase four-wire distribution systems. In Proceedings of the 2011 IEEE Power and Energy Society General Meeting, 2011; pp. 1–7.
23. Wang, K.; Skiena, S.; Robertazzi, T.G. Phase balancing algorithms. *Electr. Power Syst. Res.* **2013**, *96*, 218–224. [CrossRef]
24. *IEC 61000-2-2*; Electromagnetic Compatibility (EMC)-Part 2-2: Environment-Compatibility Levels for Low-Frequency Conducted Disturbances and Signalling in Public Low-Voltage Power Supply Systems. Standard, International Electrotechnical Commission (IEC), International Electrotechnical Commission: Geneva, Switzerland, 2002.

25. Girigoudar, K.; Molzahn, D.K.; Roald, L.A. On the Relationships Among Different Voltage Unbalance Definitions. In Proceedings of the 2019 North American Power Symposium (NAPS), Wichita, Kansas, 13–15 October 2019; pp. 1–6. [CrossRef]
26. IEEE. *IEEE Recommended Practice and Requirements for Harmonic Control in Electric Power Systems*; Standard; IEEE Standards Association: New York, NY, USA, 2014.
27. Elkhorchani, H.; Grayaa, K. Novel home energy management system using wireless communication technologies for carbon emission reduction within a smart grid. *J. Clean. Prod.* **2016**, *135*, 950–962. [CrossRef]
28. Kütt, L.; Saarijärvi, E.; Lehtonen, M.; Mõlder, H.; Niitsoo, J. A review of the harmonic and unbalance effects in electrical distribution networks due to EV charging. In Proceedings of the 2013 12th International Conference on Environment and Electrical Engineering, Wroclaw, Poland, 5–8 May 2013; pp. 556–561.